Chapter 4

Noble Metal Dispersed on Reduced Graphene Oxide and Its Application in PEM Fuel Cells

Adriana Marinoiu, Mircea Raceanu, Elena Carcadea, Aida Pantazi, Raluca Mesterca, Oana Tutunaru, Simona Nica, Daniela Bala, Mihai Varlam and Marius Enachescu

Additional information is available at the end of the chapter

http://dx.doi.org/10.5772/intechopen.80941

Abstract

Metal-dispersed nanoparticles on reduced graphene oxide as catalyst for oxygen reduction reaction (ORR) demonstrate promising applications in the energy sector. The catalyst activity enhancement and stability improvement investigated in this study are mandatory steps in obtaining feasible electrodes for PEMFC. The chapter deals with the synthesis of noble metal catalysts including platinum and gold nanoparticles dispersed on reduced graphene oxide (PtNPs/rGO and AuNPs/rGrO). The understanding of the correlations between the electrochemical activity on one side and the structure, composition and synthesis method on the other side are provided. Facile routes in order to prepare the well dispersed PtNPs/rGO and AuNPs/rGrO are included. The structure and morphology were characterized by different techniques, namely X-ray diffraction (XRD), Scanning Transmission Electron Microscopy (STEM), specific surface area measurements. In this context we report a hybrid derived electrocatalyst with increased electrochemical active area and enhanced mass-transport properties. The electrochemical performances of PtNPs/rGO and AuNPs/rGrO were tested and compared with a standard PEMFC configuration. The performed electrochemical characterization recommends the prepared materials as ORR electrocatalysts for the further fabrication of cathodes for PEM fuel cells. The research directions as well as perspectives on the subsequent development of more active and less expensive electrocatalysts are established.

Keywords: fuel cell, cathode, doped graphenes, oxygen reduction reaction

1. Introduction

Almost 60 years have passed from Feynman's famous and incredible visionary talk "There is plenty of room at the bottom" and many of his statements are the reality today. The new field he was just introducing was defined as having an enormous number of technical applications. And so right he was! In this chapter, we are going to discuss one of those applications. Fuel cells are among the major scientific discoveries that had a strange "life". Despite their modern tech aura, the wonderful discovery of Mr. Grove, 150 years ago, had in the last 20 years an extremely variable popularity, reaching their peak at the end of the last century, when scientists and stock promoters envisioned a world run on clean and inexhaustible resource—hydrogen. At that time, it was predicted that soon, cars will run on fuel cells and households will generate electricity from back-yard fuel cells. Improvements in stack design during that time led to increased power densities and lower costs. However, high manufacturing costs, marginal performance and short service life stood in the way of turning the hydrogen dream into reality. Nowadays, a new "wave" has emerged, partly due to exactly the new field introduced by Mr. Feynman—nanostructure-based catalysts.

The development of human society requires more resources to meet the enhanced energy demand of society. With the rapid increase in energy demand in people's everyday lives, research into new environment-friendly energy sources and their practical applications have attracted increasing attention. Fuel cells demonstrated important advantages with distinguishing features compared to conventional power sources, such as internal combustion engines or batteries, namely: higher efficiency and silent operation in comparison to internal combustion engines; no pollution considering the only by-product at the point of use is water; the maintenance of fuel cells is simple; low temperature proton exchange fuel cells (PEMFC) have low heat transmission; operating time is much longer than in the case of batteries, since doubling the operating time needs only doubling the content of fuel and not the doubling of the capacity of the unit itself; as opposed to batteries, fuel cells have no "memory effect" when are replenished.

The main advantages of new nanostructured materials are their very high surface area to volume ratio and high absorption rates. There are nanoscale materials of various types, including nanoparticles, nano-powders, nano-rods, nanotubes, and nanowires. It is well known that nanomaterials have multiple dimensionalities, including zero dimensional, 1-D, 2-D and 3-D. One dimensional materials are widely used in various applications because of their high surface area and porosity. Carbon-type materials are known to have good features, such as abundance, stability, environmental safety and high durability. They exhibit high chemical stability over a wide temperature range in both acidic and alkaline conditions, making them the most suitable candidates for electrodes in electrochemical energy devices. There are many available carbon allotropes, such as buckminster fullerenes, carbon nanotubes, graphene and nano-diamonds. In the last years, graphene is considered as a major material in energy conversion and storage applications in general and in PEM fuel cells topic particularly. Therefore, one of the cornerstones of the push towards future improvements in present-day PEM fuel cell, and the research and development generated by this push, is the introduction of nanostructured catalysts in order to mitigate the main issues of the technology—high prices and low service life.

PEMFC cells are currently the leading technology for light duty vehicles and in a smaller proportion for stationary and other applications. Commercialization of light duty FC vehicles started recently. The market for FC vehicles is still limited to the present day, mainly due to an insufficient hydrogen fueling infrastructure, but also to a considerable cost of FC systems able to achieve the target lifetime [1, 2]. For example, it is recognized that a decrease in platinum loading has a negative impact in respect to durability. In this particular domain of catalyst durability for FC systems the smetal-dispersed nanoparticles can concurrently lower the catalytic system cost playing a significant role in technology developments in the near future [3]. Moreover, most of the researches have been devoted to reduce the resistance of the electrolyte membrane by lowering the thickness, which caused inferior mechanical properties of the thinned membrane.

The total cost of a fuel cells stack can be greatly reduced by reducing the catalyst load and using low- or non-Pt-based electrocatalysts. Therefore, the ways to improve the catalytic activity and reduce the cost of anodic and cathodic catalysis are critical issues to achieve the real fueling of the fuel cells. In PEM fuel cells, the efficiency of the cathode electrocatalyst plays an important role in increasing energy conversion efficiency and achieving higher power densities. In recent years, new 3D graphene-based materials have been developed, that have proved to be effective electrocatalysts for ORR [4]. The main directions for increasing the catalytic activity and reducing the production costs for the ORR catalysts were as follows: the development of nano-graphene nanostructures based on noble metals, either by doping with non-metals or by the deposition of non-metallic nanoparticles or metallic oxides with a catalytic role; decreasing the noble metal content of the electrocatalyst.

In recent years, various catalyst support materials have been proposed to meet the challenges. In addition to traditional carbon materials, non-carbon materials such as metal oxides, electroconducting polymers, carbides, nitrides, etc. have been proposed and sustained as catalysts. The nanostructured materials meet the requirements of a high-surface catalyst with high active surface sites and a low metal load. Consequently, a number of non-metallic catalysts have been developed, but the catalytic performance has been modest [5, 6]. The ORR reaction at the cathode plays a critical role in the performance of a fuel cell. Although substantial advances have been made in cathodic catalysis over the last decades, the slow kinetics of ORR electron transfer and overpotential are the disadvantages that limit the large-scale marketing of PEMFC.

The porous graphene has remarkable properties for electrochemical power systems [7]. In general, nanoelectrocatalysts based on graphene used in PEMFC can be classified into the following types, depending on the composition of the catalysts: (1) Pt-based nanocatalysts supported on graphene; (2) noble metals supported on graphene as electrocatalysts, including transition metals and their oxides, sulphide nanomaterials and metal complexes (3) Pt-free graphene-supported electrocatalysts, including alloys Pd, Au, Ag and nanomaterials; and (4) non-metal electrocatalysts, including surface functionalized graphene and heteroatom doped graphene. It should be noted that, despite the substantial advances made in the construction of advanced electrocatalysts based on graphene and the understanding of their electrocatalytic mechanism, a number of scientific and technical challenges still remain in order to achieve the commercialization of graphite-supported electrocatalysts in fuel cells. It is anticipated that graphene support nanomaterials are a promising class of fuel cell electrocatalysts.

The catalytic activity of the Pt graphene composites can be improved by increasing the charge transfer from the catalysts to the graphene substrate. The chemically functionalized graphene with interlayer structure contains network defects (bare spots, holes) and surface functional groups (carbonyls, epoxies, hydroxyls, etc.) that can bind metal nanoparticles and can retain them on the graphene surface. A strong metal–substrate interaction was demonstrated to enable the stability of the nanocatalyst, which can be improved by dispersion. Using Density Functional Theory (DFT) it was found that surface defects in the graphene support can also act as strong traps for Pt nanoclusters, leading to long-term stability of Pt graphene composites.

Metallic graphene hybrids have exhibited significant electrocatalytic activities when used as anodic and cathodic catalysts in PEM fuel cells. Both n- and p-type conductivities can be obtained by selecting metal dopants, and the carrier concentration can be controlled by the quantity of metal deposited [8]. For example, several transition metals with different work functions, such as Ti, Fe, Cu, Ag, Au, and Pt, have been used for graphene band modulation. In particular, band arrangement is not only determined by work function, but also affected by the interfacial interactions, as a consequence the metal structures would influence the charge transfer between metal and graphene. Moreover, first-principles calculations indicated that the carbon-vacancies attract and trap metal atoms [8]. The binding of a single metal atom nearby a single-vacancy (SV) on the graphene was investigated recently for Pt, Pd, Au, and Sn, using the density-functional theory (DFT). Regarding the pristine graphene, Pt, Pd, and Sn prefer to be adsorbed at the bridge site, while Au prefers the top site. On the single-vacancy graphene, all the metal atoms prefer to be trapped at the vacancy site and appear as dopants. The trapping abilities of the SV-graphene for different metal atoms, are different, that is, the Pt and Pd have the larger trapping zones. The diffusion barrier of a metal atom on the SV-graphene is much higher than that on the pristine graphene, and the Pt atom has the highest diffusion barrier from the SV site to the neighboring bridge sites. More electrons are transferred from the adatoms (or dopants) to the carbon atoms at the defect site, which induces changes in the electronic structures and properties of the systems. However, the Pt atom is easier to be incorporated into the SV-graphene [8].

In our previous efforts on the development of innovative fuel cell catalysts, an experimental approach of finding low cost alternative support material in PEMFC was developed [9]. The potential of using graphene oxide as support/catalyst for PEMFC was exploited. Moving forward, Pt/graphene nanocomposites were synthesized using a simple route involving chemical oxidation, exfoliation of graphene oxide, as well as functionalization with a compatible polymer. Poly-diallyldimethylammonium chloride (PDDA) was used as cationic polyelectrolyte, with ability of adsorption on the graphene surface through π–π and electrostatic interactions, acting as a stabilizer for controlled synthesis of Pt/graphene [9, 10].

2. Experimental

2.1. Synthesis of graphene: noble metals nanocomposites

Graphite powder, $K_2S_2O_8$, P_2O_5, conc. H_2SO_4, $KMnO_4$, HI were purchased from Sigma-Aldrich, H_2O_2 and HCl were obtained from Oltchim SA Romania. The electrocatalysts were synthesized

http://dx.doi.org/10.5772/intechopen.80941

via a facile process (**Figure 1**) described in detail elsewhere [11, 12]. Graphite oxide was prepared by the oxidation of graphite powder using P_2O_5, H_2SO_4, and $KMnO_4$ according to the Hummers' method, namely the graphitic powder was mixed with an oxidizing agent, filtered, washed and dried. Graphite oxide was dispersed in water by sonication for 2 h, forming the stable graphene oxide suspension (GO). Then, solutions of NaCl and the precursor of corresponding metal (water solutions of H_2PtCl_6 or $HAuCl_4$) were added individually to GO suspension under continuous mechanical stirring (500 rpm for 1 h).

Freshly prepared solution of $NaBH_4$ was added slowly to the reaction mixture under vigorous stirring. The reaction mixture was stirred for another 24 h for the complete reduction, then washed with large amount of water several times, separated by filtration and centrifugation in order to remove residual ions. The obtained mass was then dried. pH plays an important role in the obtaining of the metal dispersed rGO, therefore the values of this parameter were mentioned in the experimental part (**Figure 1**) during each proposed fabrication steps. Aqueous NaOH and HCl solutions were used to adjust the pH value. In this work, we took into consideration the preparation of highly dispersed platinum and gold nanoparticles on reduced Graphene Oxide nanosheets with different metal compositions: Pt/rGO_x and Au/rGO_y. It is known the fact that, during reduction step, graphene oxide gradually loses its oxygen-containing groups and could become hydrophobic, thus a direct reduction without a compatible polymer with ability of adsorption on the graphene surface, generally causes irreversible agglomerations. In our developed protocol synthesis PDDA was used as cationic polyelectrolyte owing to its expected reason of stabilizer effect, favoring the electrostatic interactions. Therefore, the bonding of reduced graphene oxide (rGO) with PDDA offers the possibility of controlling the behaviors of RGO in suspensions.

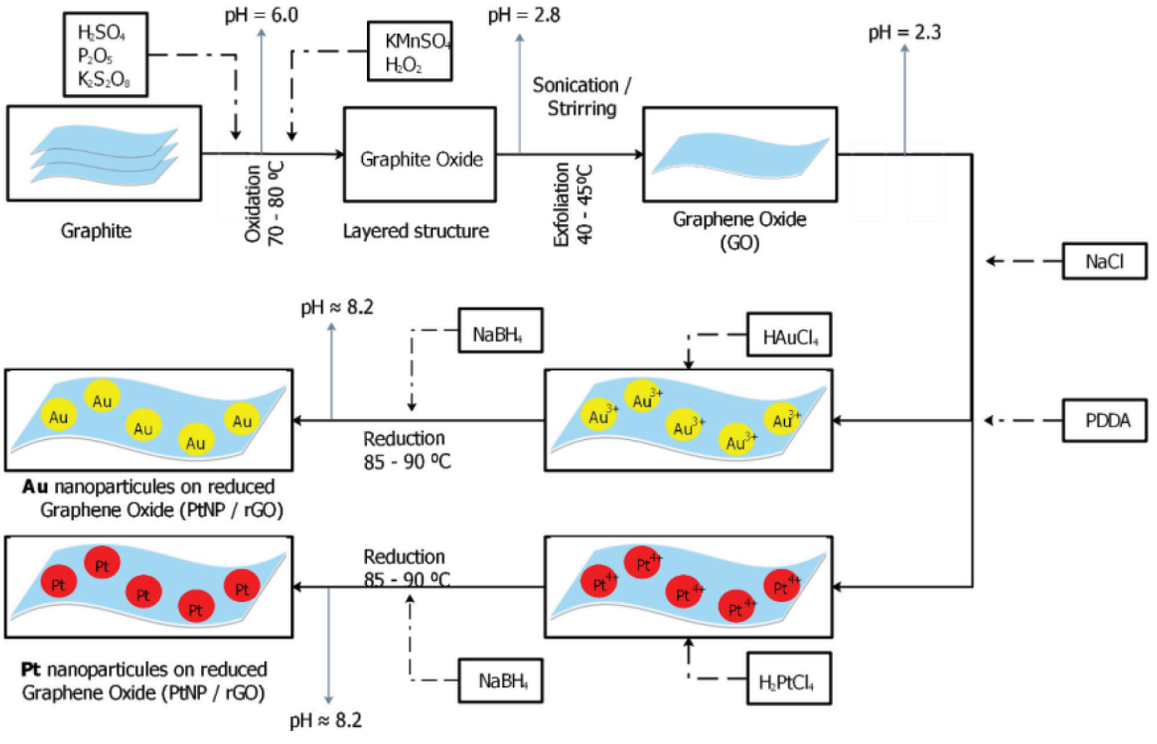

Figure 1. Reaction routes for the synthesis of metal nanoparticles on graphene oxide.

2.2. Catalysts characterization

The microstructure and morphology of prepared samples were evaluated by using the following techniques: Scanning Electron Microscopy (SEM), Scanning Transmission Electron Microscopy (STEM), specific surface area. Scanning Electron Microscopy (SEM) measurements were carried out using a Hitachi SU 8230 Scanning Electron Microscope equipped with EDS detector-analyzer. Hitachi HD 2700 Scanning Transmission Electron Microscope equipped with EDX Oxford detector-analyzer was used to perform graphene samples analysis. For the analysis, the samples in the form of powder were dispersed in bi-distilled water using a probe-type ultrasonic homogenizer and deposited on a standard Cu TEM grid. Also, EDX analysis was performed to determine the chemical composition of the samples. Autosorb IQ (Quantachrome, USA) instrumentation was used to perform the adsorption and desorption experiments at 77 K after initial pre-treatment of the samples by degassing at 115°C for 4 hours. The powder X-ray diffraction (XRD) analyses were performed at room temperature on a Rigaku SmartLab X Ray Diffractometer with Cu target $K_{\beta 1}$ = 1.39217 Å, $K_{\alpha 1}$ = 1.540598 Å and $K_{\alpha 2}$ = 1.544426 Å. The diffraction data was recorded for 2θ angles using the following parameters: tube voltage = 45 kV, tube current = 200 mA, scan range: 5–90°. The identification of the phase was made by referring to the International Center for Diffraction Data—ICDD (PDF-2) database.

2.3. Electrode preparation and electrochemical measurements

The modified carbon paste electrodes were prepared by mixing graphite powder with paraffin oil, then mixing in a mortar until a consistent uniformly wetted paste was obtained. The ratio of the two components was approximately 3:2 (w/w). The obtained paste was placed into a plastic syringe with an inner volume of 1.0 mL. The electrical contact was assured by a copper wire that was inserted into the back of the graphite paste. The modified electrodes were prepared by mixing certain amounts of carbon paste with platinum-doped reduced graphene oxide and gold-doped reduced graphene oxide in ratio of 109.7:0.3 and 109:1 (w/w), respectively. The obtained materials were pressed at the end of carbon paste from syringes. Thus, four electrodes were prepared: bare carbon paste electrode (CPE), graphene oxide modified carbon paste electrode (denoted by GO), platinum-doped reduced graphene oxide (denoted by Pt/rGO) and gold-doped reduced graphene oxide (denoted by Au/rGO). The surface of all electrodes was smoothed by polishing on a piece of weighing paper. Electrochemical measurements were carried out on a potentiostat/galvanostat system AutoLabPGStat 12, controlled by GPES (general purpose electrochemical system), electrochemical interface for Windows (version 4.9.007). Three electrodes in one compartment cell (10 mL) were used in all experiments. A glassy carbon electrode (Metrohm, 3 mm in diameter) and each modified carbon paste electrodes served as working electrodes. The counter electrode was a large area Pt wire. All experimental potentials were referred to Ag/AgCl, KCl_{sat} as reference electrode.

The electrochemical characterization of the modified carbon paste electrodes was carried out by cyclic voltammetry (CV) and differential pulse voltammetry (DPV). The CV experiments were recorded in 0.5 M KCl solution containing 1.0 mmol L^{-1} $K_3Fe(CN)_6$ in the potential range of (−0.35) to (+0.8) V at scan rates of 20–120 mV s^{-1}. DPV curves were recorded in the same potential domains with 5 mV potential and 25 mV as modulation amplitude.

http://dx.doi.org/10.5772/intechopen.80941

3. Results and discussions

Firstly, the characterization of the prepared materials was performed to validate the microstructural quality and to confirm the metal presence and the structured morphology (**Figures 2** and **3**).

The crystalline structure of Pt/rGO_x and Au/rGO_y composites was characterized by X-ray diffraction (XRD). XRD patterns of prepared doped-graphene with Pt or Au nanoparticles are presented in **Figure 4**. The prepared materials exhibited characteristic diffraction peaks at 39.76° (38.18°), 46.24° (44.39°), 67.46° (64.58°), 81.29° (77.55°)corresponding to the (111), (200), (220), (311) planes of face-centered cubic structure of Pt (PDF Card 00-004-0802) and Au (PDF Card 00-004-0784), respectively. The diffraction peaks in all samples are also assigned to the structure of the graphene oxide support.

Based on the intensity of the main peaks from the XRD patterns and using on the Scherrer's equation, the mean crystallites sizes were computed: $D_{hkl} = K\lambda/B_{hkl}\cos\theta$, where D_{hkl} is the crystallite size in the direction perpendicular to the lattice planes (hkl), K is a constant related to crystallite shape, λ is the X-ray wavelength in nm, and B_{hkl} is the peak width at half-maximum peak height. The crystalline size estimated from the Scherrer equation is between 14 and 25 nm for Au/rGO and 7–15 nm for Pt/rGO.

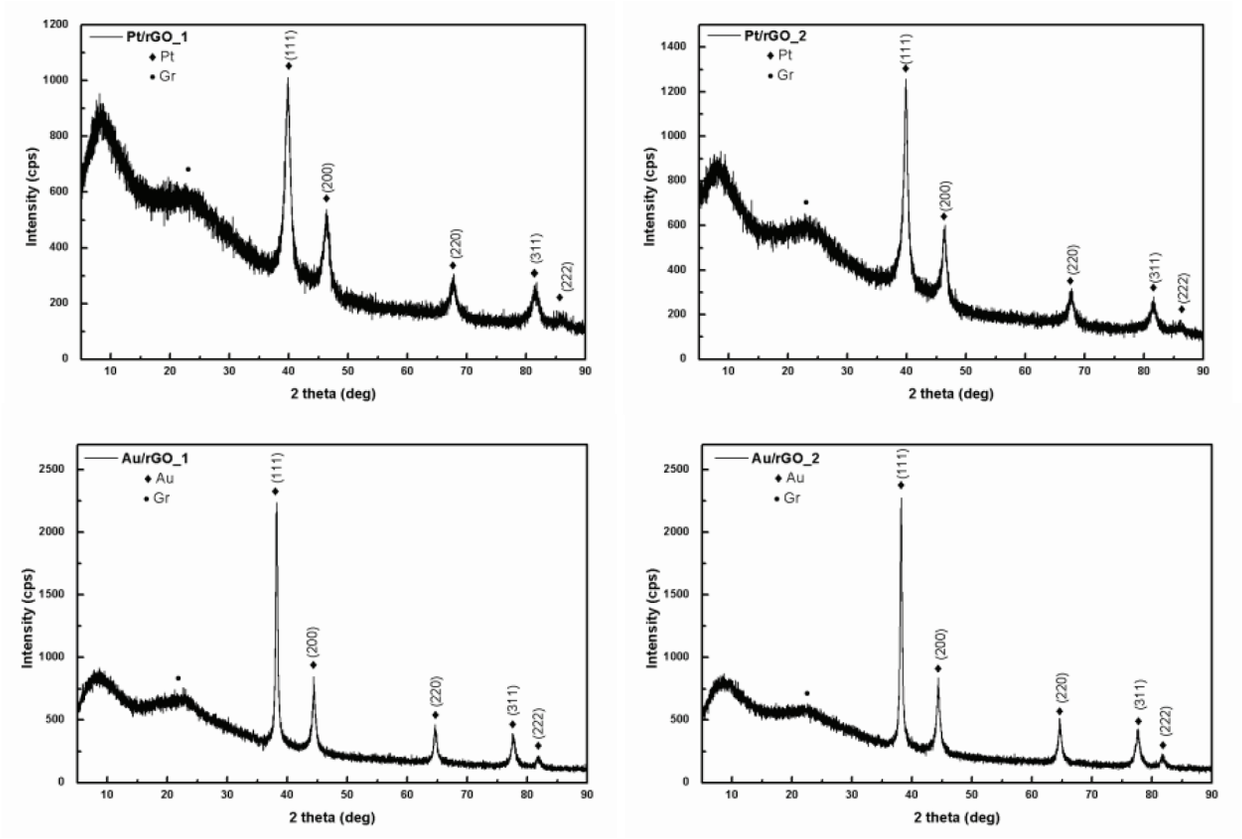

Figure 2. XRD patterns of metal-dispersed nanoparticles on reduced graphene oxide composites: Pt/rGO—up and Au/rGO—down.

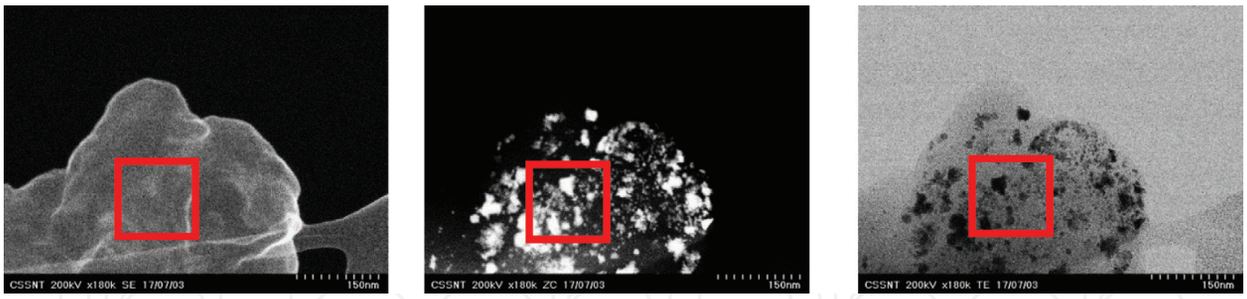

Figure 3. Co-localized SE—secondary electrons (left), ZC—phase contrast (middle) and TE—transmission electrons (right) images of the Pt/rGO_x sample.

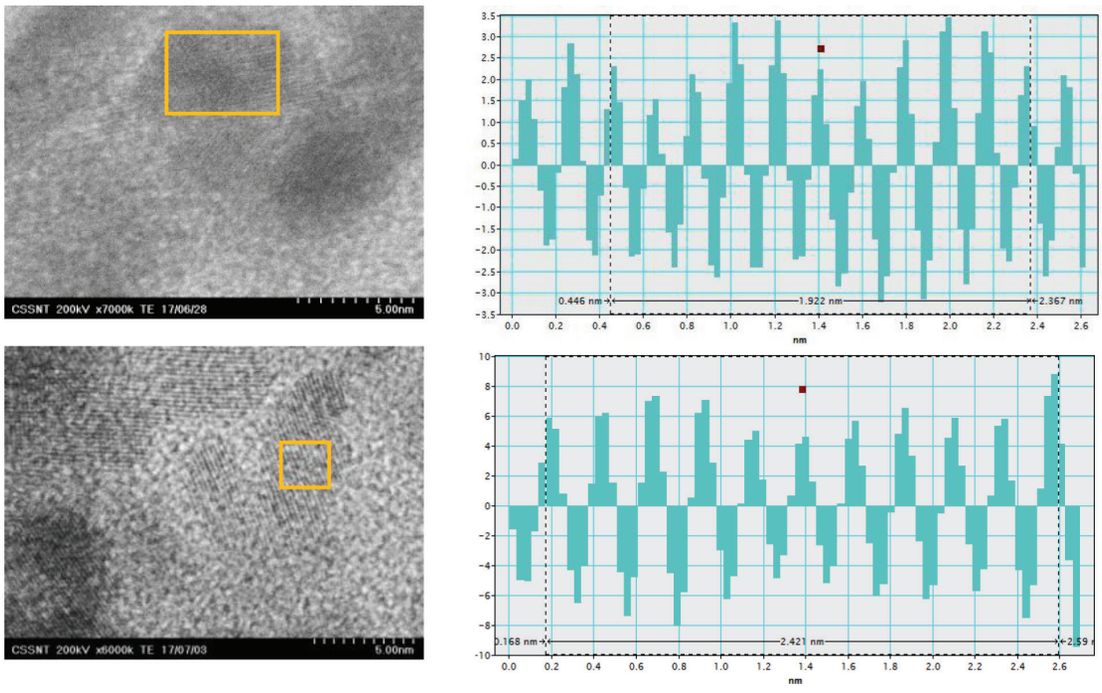

Figure 4. High resolution STEM images of the Pt/rGO_x sample were recorded in the marked area in the co-localized images from above (left). The lattice constant from the area marked in orange was measured and the resulting profiles revealed Pt and graphene specific d-spacings (right).

These obvious characteristic peaks indicate a good crystallinity of the supported Pt/Au nanoparticles in the prepared composites.

The distance between two layers is an important parameter to evaluate the structural information of graphene. Due to the presence of oxygen-containing functional groups attached on both sides of the graphene sheet and the atomic-scale roughness arising from structural defects (sp3 bonding) generated on the originally atomically flat graphene sheet the d-spacing of the GO. The rGO (002) plane was observed at 2θ of about 23° indicating interatomic spacing of about 0.384 nm.

Both metal-dispersed nanoparticles on reduced graphene oxide presented similar XRD peaks corresponding to the face-centered cubic crystalline Pt/Au and no trace of other phases was detected, suggesting that the modification of the drying conditions does not provide a major influence to the crystalline structure.

The morphology of reduced graphene oxide doped with gold or platinum samples (Pt/rGO_x and Au/rGO_y) used in this work was examined using scanning transmission electron microscopy technique and the results are shown in **Figure 5**. The images were obtained with different detectors: SE—secondary electrons (left), ZC—phase contrast (middle) and TE—transmission electrons (right) at the same location on the sample. Structural studies were performed on all samples and obtained images were almost similar for each class of materials, namely Pt/rGO_x and Au/rGO_y, respectively.

The (200) plane in Platinum Nanoparticle with face-centered cubic structure was identified with a 1.922 Å d-spacing (ideal 1.962 Å)—up. Single layer graphene flake was identified with a 2.421 Å d-spacing (ideal 2.45 Å)—down.

The (111) plane in Gold Nanoparticle with face-centered cubic structure was identified with a 2.328 Å d-spacing (ideal 2.35 Å)—up. Single layer graphene flake was identified with a 2.461 Å d-spacing (ideal 2.45 Å)—down.

Figures 5 and **6** show the high resolution STEM micrographs, in which the interplanar distances can be clearly seen. The as marked interplanar distances are inserted in profiles from the orange marked areas, corresponding to the (111) and (200) face-centered cubic structure of Pt and Au, respectively, which is in agreement to XRD results.

STEM images showed the Pt and Au nanoparticles supported on the rGO as well-dispersed and well-separated metal nanoparticles, indicating a good spatial distribution of metal nanoparticles on the layered graphene sheets.

The Energy-Dispersive X-ray spectra (EDX) were measured to characterize the elemental heterogeneity of PtNP/rGO_x and AuNP/rGO_y composites. The quantitative analysis was performed at 400x magnification. The EDX spectra for PtNP/rGO_x show signals for carbon, oxygen and platinum with composition presented in **Table 1**. The EDX spectra for AuNP/rGO_y, present signals for carbon, oxygen and gold with composition presented in **Table 2**.

With the desirable structural information presented so far, the materials with higher metal content, were further characterized and tested.

The doping of Pt/Au into graphene oxide is expected to produce some changes in surface area and consequently to the pore size. Thus, due to the porous appearance of the materials confirmed by the performed analysis and taking into account the need for a high surface

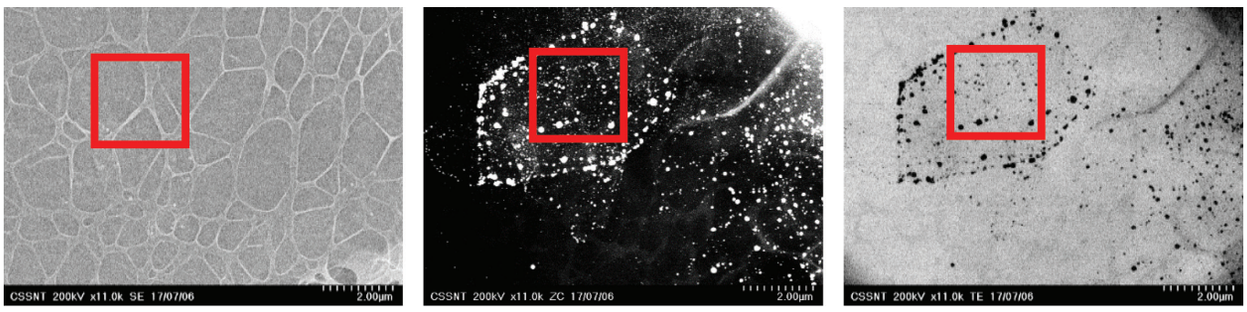

Figure 5. Co-localized SE—secondary electrons (left), ZC—phase contrast (middle) and TE—transmission electrons (right) images of the Au/rGO_y sample.

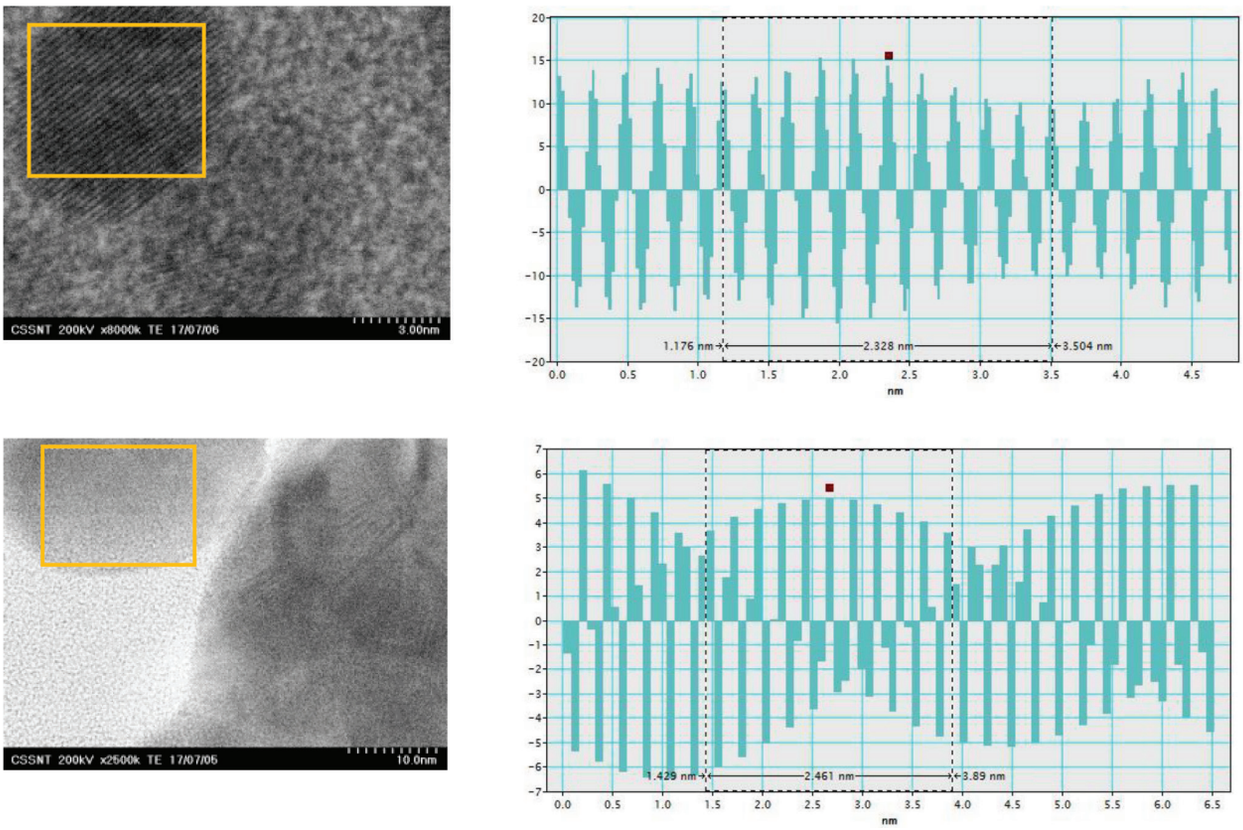

Figure 6. High resolution STEM images of the Au/rGO_y sample were recorded in the marked area in the co-localized images from above (left). The lattice constant from the area marked in orange was measured and the resulting profiles revealed Au and graphene specific d-spacings (right).

Element	PtNP/rGO_1		PtNP/rGO_2	
	Weight %	Atomic %	Weight %	Atomic %
C	58.96	86.01	62.47	85.87
O	10.25	11.22	11.57	11.98
Pt	30.78	2.77	25.96	2.20

Table 1. EDAX quantitative analysis—composition profile for PtNP/rGO_y.

Element	AuNP/rGO_1		AuNP/rGO_2	
	Weight %	Atomic %	Weight %	Atomic %
C	74.91	87.16	72.75	86.46
O	13.79	12.04	14.11	12.59
Au	11.30	0.80	13.14	0.95

Table 2. EDAX quantitative analysis—composition profile for AuNP/rGO_y.

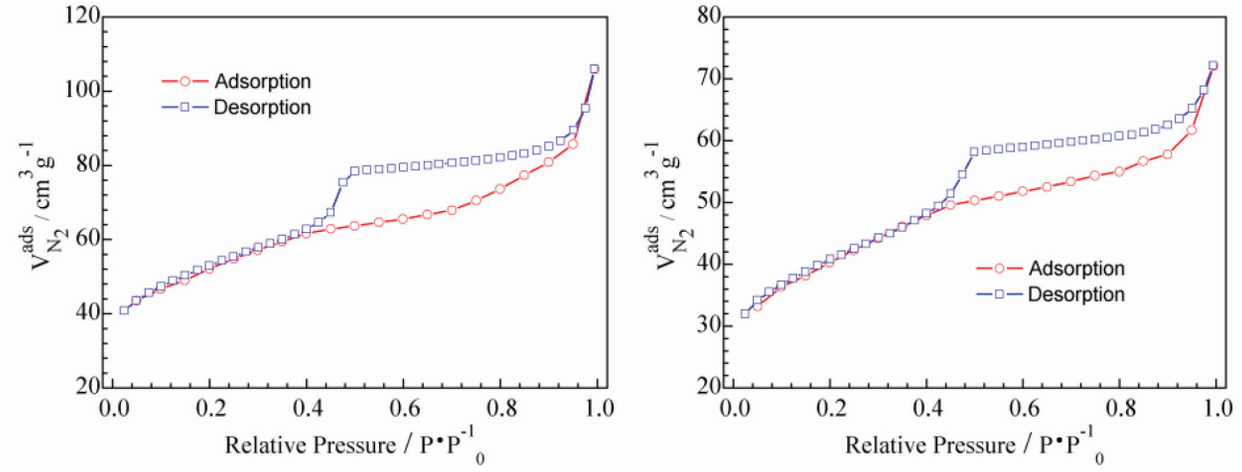

Figure 7. BET isotherms corresponding to Pt/rGO_x and Au/rGO_y.

area to provide an efficient ORR performance, we subsequently analyzed the surface area. The nitrogen adsorption–desorption isotherms were studied using Brunauer–Emmett–Teller (BET) and are provided in **Figure 7**. The hysteresis study also revealed that hysteresis loops showed parallel adsorption and desorption branches, regarded as Type H4 behavior among the IUPAC classification. This observation allows for a better understanding of the porous character of the prepared samples, demonstrating the presence of pores that are open at the end, but unconnected to each other. As shown, the isotherm curves of adsorption/desorption performance of samples were compatible with isotherm Type IV, with an abrupt increase at high relative pressure, with respect to IUPAC classification.

The BET specific surface areas are adequate, namely 158 and 107 $m^2\ g^{-1}$ for Pt- and Au-doped graphene oxide with highest metal content. Our measured surface area of the prepared doped graphene samples could be connected with the stacking structure and agglomerated morphology of the reduced graphene sheets and could be attributed to an increasing in the number of closed pores during platinum/gold doping. The estimated radii presented in **Table 3** suggest a hierarchical interconnected porous framework in the prepared doped graphene. Different pore types displayed different roles in the PEMFC electrochemical performance, thus the existence of various porous characteristics ensures sufficient space that enables the access of the reactants to the catalytic sites and could accelerate the kinetic process of ion diffusion.

Based on the structural information presented above, the prepared Pt- and Au-doped graphene oxide was evaluated as ORR cathode under practical FC operation conditions. In comparison to commercial Pt/C, a better cathode performance, including the prepared catalytic

Samples	S_{BET} ($m^2\ g^{-1}$)[a]	BJH pore volume ($cm^3\ g^{-1}$)[b]	BJH pore radius (nm)
Pt/rGO	158	0.101	1.857
Au/rGO	107	0.059	1.964

[a]BET surface area calculated from the linear part of the BET plot (P/P_0 = 0.1–0.3).
[b]BJH pore volume, taken from the volume of N_2 adsorbed at P/P_0 = 0.99, using BJH method.

Table 3. Textural properties of Pt/rGO and Au/rGO.

system based on doped graphene can be easily anticipated, taking into account our recent results [11]. This improvement in performance was explained on the basis of higher electrical conductivity and durability parameters, essential for the PEMFC commercialization.

Electrochemical processes occur at the electrode/solution interface, in contrast to many other chemical measurements that involve bulk solutions. Due to the fact that the reaction is controlled by the electrode potential, electrochemistry is very sensitive and selective for the detection of electroactive species in extremely low limits of detection (nanomolar) and very small sample volumes (μL). The material used defines the performance, hence the continuous interest in developing new generation of electrodes. Carbon materials are widely used in industrial electrochemistry and modified electrodes are still developing with the aim of enhancing both the electrochemical characteristics and performance. There is a large range of carbon based forms available for use as an electrode material, with various allotropic forms exhibiting distinct properties. Among them, graphene materials present an enormous interest for electrochemists owing to their extraordinary physical, chemical and electrical properties. Graphenes are reported as performing electrode constituents for a wide variety of electrochemical applications, including the fabrication of energy storage devices, membrane material, and simultaneous characterization of ascorbic acid, dopamine and uric acid levels [13]. Graphene is the thinnest electrode material, but there are experimental parameters to be overcome: the first problem is the electrical connection of the graphene; the second issue is to avoid the aggregation of graphene sheets to form graphite through strong π–π interactions between the constituting sheets; the last limitation regards the quality of the obtained graphenes by various routes with different electrochemical properties.

The aim of the present research is the fundamental electrochemical characterization of modified graphene-based electrode materials. In electrochemical measurements, supporting electrolytes are widely used. They contain chemical species which are not electroactive in the range of used potentials and have higher conductivity and ionic strength in comparison with electroactive species. Therefore they increase the conductivity of the solution, maintain constant ionic strength and pH, eliminate the transport of electroactive species by ion migration. KCl solutions are widely used as supporting electrolyte, due to relatively high ion conductivity; also potassium ion has a smaller hydration sphere than other alkaline ions We focused our attention on developing novel electrodes using carbon paste as support to investigations of the classical ferri/ferro redox process with attention on the electrochemistry of Pt-doped reduced graphene oxide electrodes. All the modified electrodes were tested for the redox process of 1 mM potassium ferrocyanide(II) using 0.5 M KCl as electrolyte.

$$2\,K_3[Fe(CN)_6] + 2KOH \rightarrow 2\,K_4[Fe(CN)_6] + H_2O + O \quad (1)$$

$$Fe^{3+} + e^- \leftrightarrow Fe^{2+} \quad (2)$$

The electrochemical response of a standard glassy carbon was first tested. **Figure 8** depicts the cyclic voltammetry of the ferri/ferro redox system, scanned from 20 to 120 mV/s in the −0.35 to 0.80 V potential range. The peak-to-peak separation (ΔEp) at 100 mV s^{-1} is 181 mV. Analysis of the peak-to-peak separation as a function of voltage scan rate indicates that the electrochemical process is quasi-reversible within the employed scan rates. Monitoring of the voltammetric

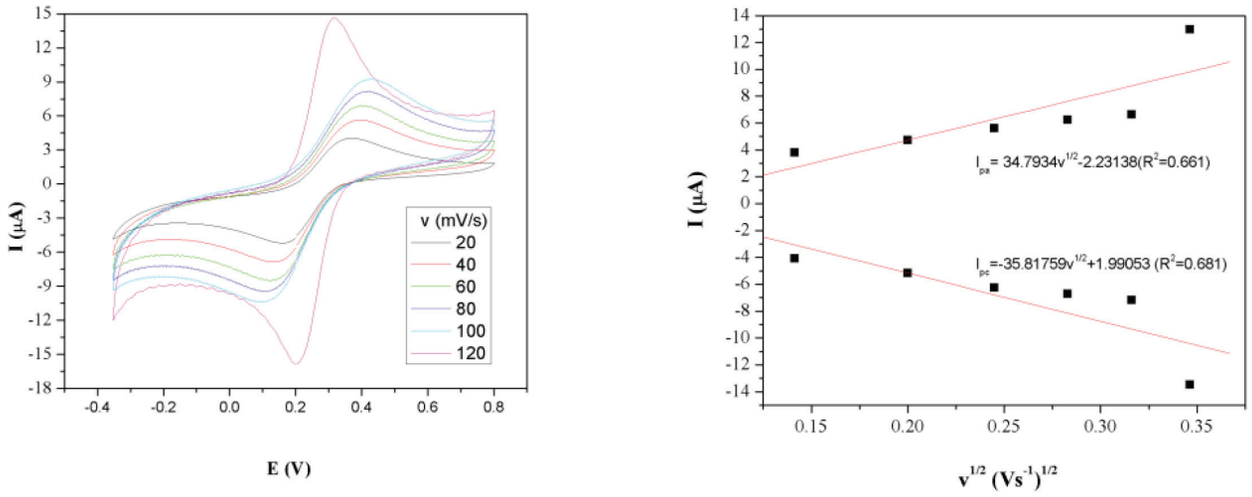

Figure 8. Cyclic voltammograms for 1.0 mM $K_3Fe(CN)_6$ in 0.5 M KCl solution on glassy carbon electrode, v = 20–120 mV s^{-1} (left) and plot of I *vs*. $v^{½}$ (right).

peak height as a function of the square-root of scan rate shows a highly linear response, indicating a diffusion electrochemical process in accordance with reported literature data [14].

The focus herein is to electrochemically characterize reduced GO modified electrodes for efficiency towards ferri/ferro redox probe. For achieving this goal, carbon paste electrodes were prepared by mixing graphite powder with paraffin oil in a ratio of approximately 3:2 (w/w). The two components are hand mixed in a mortar until a consistent wet paste is formed. The obtained paste is placed into a plastic syringe with an inner volume of 1.0 mL. For assuring the electrical contact, a copper wire was inserted into the back of the carbon paste. A control experiment was first performed utilizing a bare carbon paste electrode. The electrochemical characteristic signatures are similar with those of the glassy carbon, the peak-to-peak separations (ΔEp) at 100 mV s^{-1} being 325 mV. This, together with smaller intensity of the peaks indicates that the bare carbon paste electrode is not sensitive to the chosen redox probe. However, the electrochemical process is also diffusion controlled, the voltammetric peak height as a function of the square-root of scan rate also showing a linear response (**Figure 9**).

Next, the modified electrodes were prepared by mixing certain amounts of carbon paste with graphene oxide and then, carbon paste with metal-doped graphene oxide. We have previously observed that modified gold-doped reduced graphene oxide electrodes are sensitive for ferri/ferro redox systems. In all cases, the surface of the electrodes was smoothed by polishing with filter paper. All electrodes were kept in distilled water before and after measurements. The electrochemical measurements were carried out on a potentiostat galvanostat system using one compartment cell of 10 mL containing three electrodes. Each modified carbon paste electrode served as working electrodes. The counter electrode was a large area Pt wire and Ag/AgCl, KCl_{sat} constituted the reference electrode. The experiments were run in the potential range of −0.35 to 0.8 V at various scan rate.

To ensure a better evaluation of the Pt-doped rGO modified electrode, similar experiments with GO-modified electrode were performed. By comparison with the bare carbon paste electrode, the experimental results showed better defined anodic and cathodic peaks related

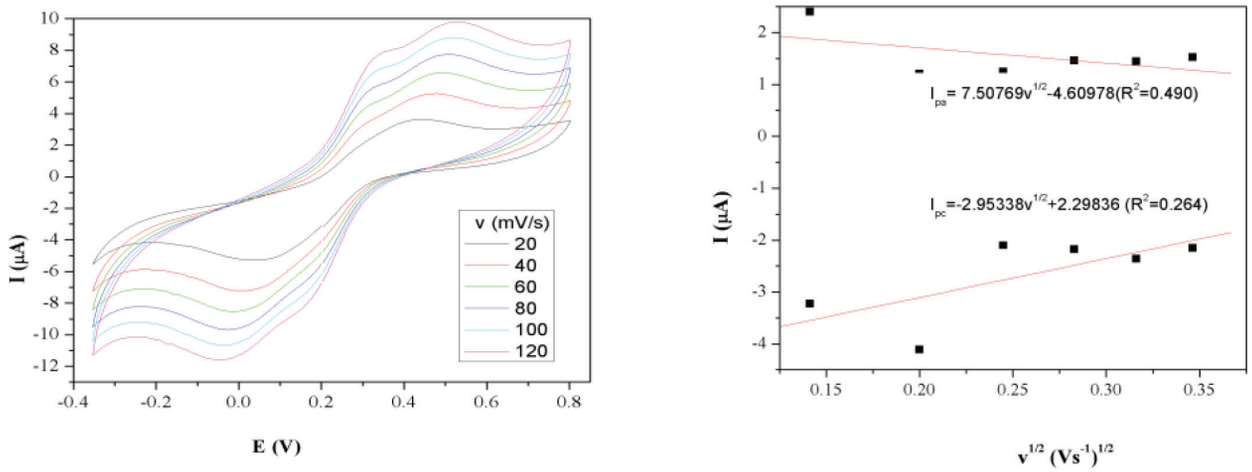

Figure 9. Cyclic voltammograms for 1.0 mM $K_3Fe(CN)_6$ in 0.5 M KCl solution on bare carbon paste electrode, v = 20–120 mV s^{-1} (left) and I *vs*. $v^{½}$ plot (right).

to $Fe(CN)_6^{3-}/Fe(CN)_6^{4-}$ redox couple for slow (20 mV/s) and high scan rates (100 mV/s) (**Figure 10**). The peak separation potential ΔEp was observed as 182 mV, similar with the results observed for the standard glassy carbon electrode. A comparison of cyclic voltammetry measurements is presented in **Figure 11**. In the case of the GO-modified electrode, for both slow and fast sweep rates, both the anodic and the cathodic peaks are sharper and well defined when compared to bare carbon paste electrode. This highlights the positive effect of the graphene oxide on the carbon paste support used for the preparation of the modified electrodes, an improvement of the analytical signal (peak height) being clearly observed.

The voltammetric profile of GO modified electrode was next explored by sweep rate variation from 20, 40, 80 to 120 mV/s. The results show that the anodic peaks increases with increasing the sweep rate and moves to positive potentials. Also, by increasing the sweep rate, the peak shape does not modify, which leads to the conclusion that this modified electrode is sensitive for the electrochemical investigation of the ferri/ferro process. Analysis of the voltammetric peak height as a function of the square-root of the scan rate reveals a highly linear response as observed for the above two investigated electrodes.

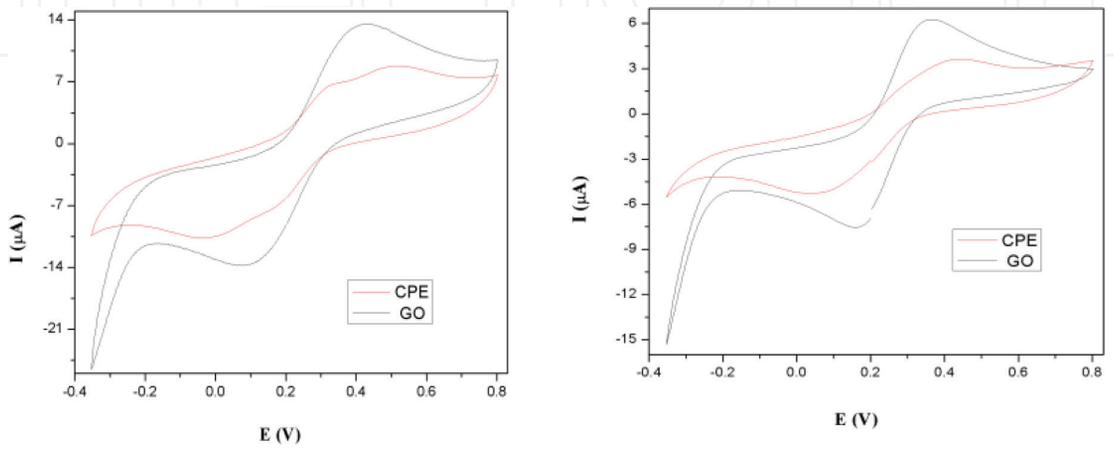

Figure 10. Comparison of the cyclic voltammograms of the modified electrodes according to the legends performed at 20 mV/s (left) and 100 mV/s (right) scan rate.

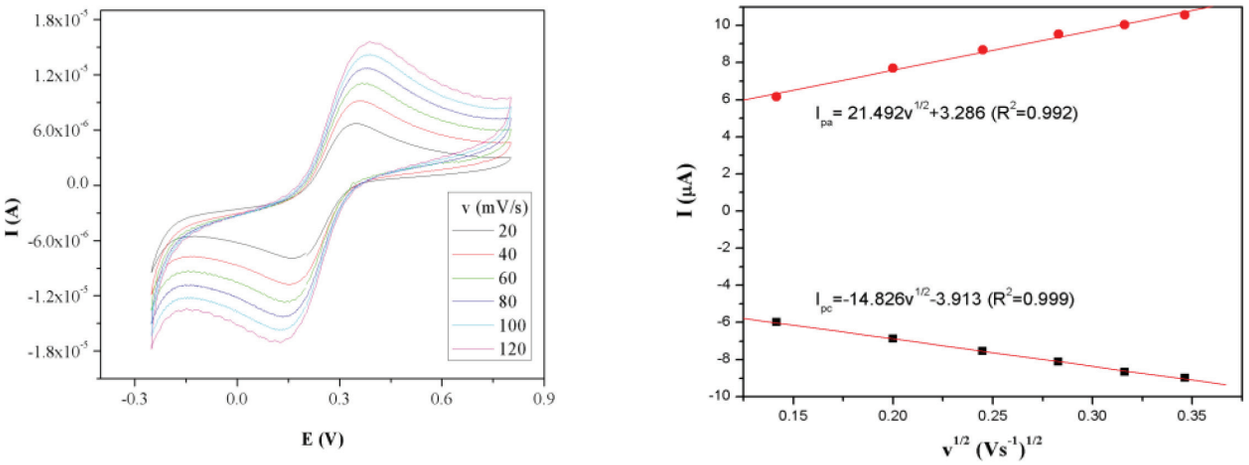

Figure 11. Cyclic voltammograms for 1.0 mM $K_3Fe(CN)_6$ in 0.5 M KCl solution on GO modified electrode, v = 20–120 mV s^{-1} (left) and I *vs.* $v^{½}$ plot (right).

Owing to the superior electrochemical response of the GO-modified electrode, we further explored whether the introduction of metal-doped rGO onto the carbon paste modified electrodes improves the electrochemical response of the studied redox system. Thus, we studied the Pt-doped rGO modified electrode. **Figure 12** shows an overlay of the cyclic voltammograms of Pt/rGO and GO modified electrodes. Analysis of the cyclic voltammograms reveals that the platinum-doped rGO modified electrode exhibits an enhancement of the current response when compared to GO which translates in better electrocatalytic activity for both oxidation and reduction processes, due to the metal presence. A better electrochemical performance than the non-metal modified GO electrode was recorded with a current 3.94 times higher than bare carbon paste electrode (**Table 4**). Both anodic and cathodic peak potentials

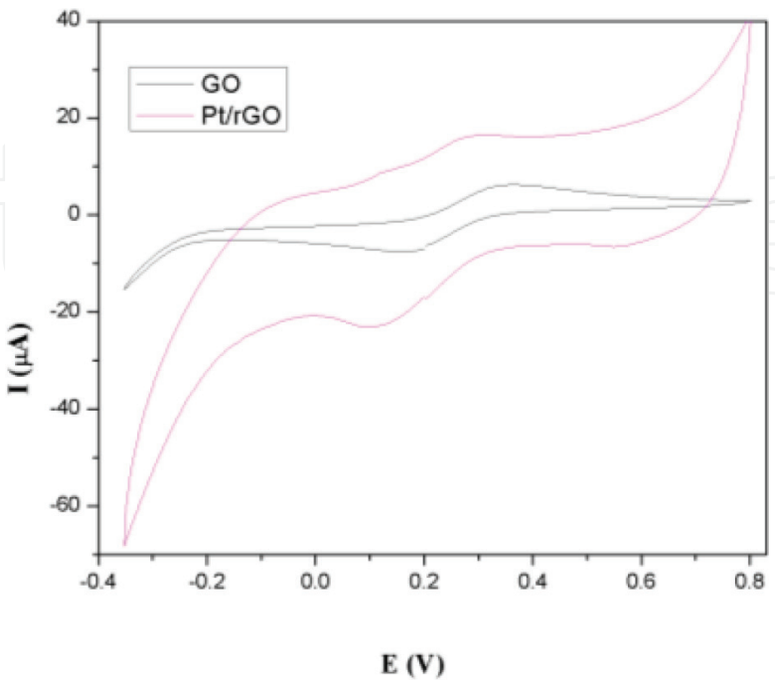

Figure 12. Overlay of the cyclic voltammograms for GO and Pt-doped rGO modified electrodes for the redox process of 1.0 mM $K_3Fe(CN)_6$ in 0.5 M KCl solution (v = 20 mV s^{-1}).

Entry	Electrode type	I_a (A)	I_c (A)	ΔE (mV)	A (cm^2)
1.	CPE	$2.40 \cdot 10^{-6}$	$-3.23 \cdot 10^{-6}$	325	0.0165
2.	GO	$6.14 \cdot 10^{-6}$	$-5.99 \cdot 10^{-6}$	182	0.0309
3.	Au/rGO	$9.45 \cdot 10^{-6}$	$-1.47 \cdot 10^{-5}$	200	0.2020
4.	Pt/rGO	$5.01 \cdot 10^{-6}$	$-8.04 \cdot 10^{-6}$	153	0.0660

Table 4. Electrochemical data from CV measurements at 20 mV/s; I_a and I_c represent the anodic and cathodic peak currents, ΔE is the separation between the peak potentials and A is the area of an electrode, with the corresponding measurements units.

are shifted by approximately −80 mV for Pt/rGO, when compared with the potential of bare carbon paste electrode. An increase in the peak currents and a decrease in the separation between the peak potentials (ΔEp) at 20 mV s^{-1} were observed for all modified electrodes in comparison to the bare CPE (ΔEp = 385 mV), indicating that the electron transfer reaction was kinetically and thermodynamically favored at the graphene oxide modified electrode surface.

By increasing the scan rate, the intensity of the peak increases not only in the anodic direction, but also in the cathodic side. The peaks are not well defined, most likely because of the low concentration of the platinum-doped reduced graphene oxide in the modified electrode. The effect of varying the scan rate results in the slight shifting of the peak potentials to higher values, indicating a quasi-reversible electron transfer. The plot of the peak height *vs.* square-root of the scan rate is illustrated in **Figure 13**, on the right. Both, the anodic and the cathodic peak currents reveal linear response at all scan rates with very good correlation factors above 0.9. These results indicate that the electrochemical process is, as previously observed, controlled by the diffusion of the electroactive species. Modified electrodes containing platinum-doped graphene materials cause an increase of the current, however due to the low concentration, the peaks are not well defined. Reported literature data showed that the electrochemical response of graphene modified electrodes can be improved by increasing the amount of graphene into the electrode [15]. The electrochemical data and areas of the electrodes presented in **Table 4** reveal that the Pt-doped rGO modified electrode has a higher electroactive area than the graphene oxide electrode.

We have shown earlier that Au/rGO modified electrode exhibits an enhancement of the current response when compared to classical glassy carbon, which translates in better electrocatalytic activity for both oxidation and reduction processes. The Au/rGO modified electrode showed a current almost four times higher than bare carbon paste electrode.

A comparison of the cyclic voltammograms of GO, Pt- and Au-doped graphene material electrodes is shown in **Figure 14**. The cyclic voltammetric response of the gold-containing modified electrode shows well defined redox peaks with a peak-to-peak separation, ΔE, of 200 mV. Thus, it was clearly revealed that the insertion of gold onto the modified graphene oxide electrodes gives improved electrochemical response for the ferri/ferro redox signal.

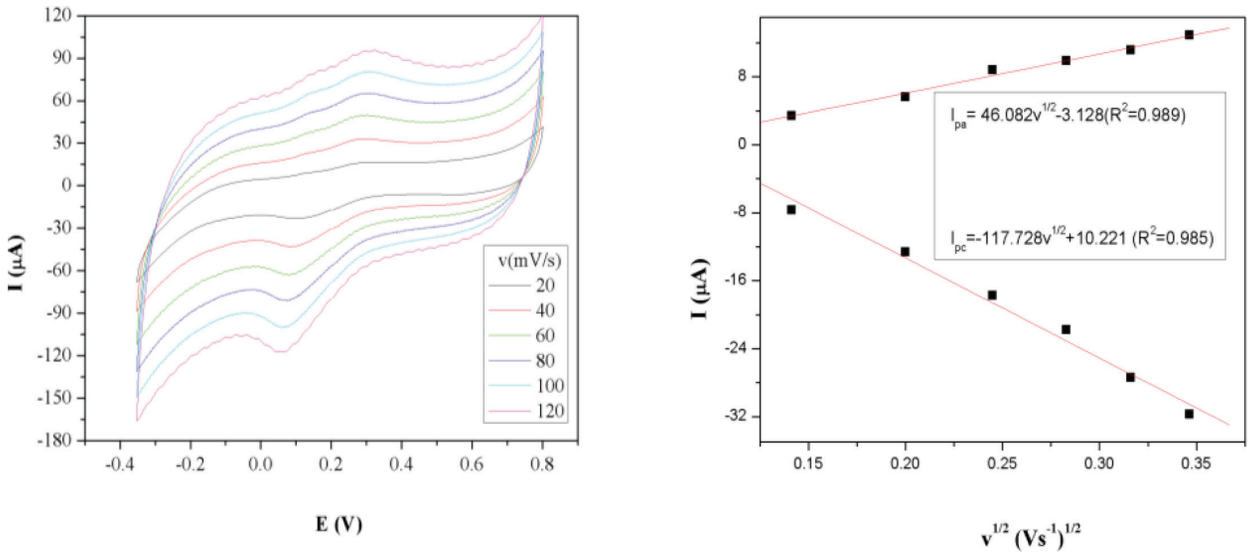

Figure 13. Cyclic voltammograms for 1.0 mM $K_3Fe(CN)_6$ in 0.5 M KCl solution on Pt/rGO modified electrode, v = 20–120 mV s^{-1} (left) and plot of I *vs*. $v^{½}$ (right).

However, the parameter of most significant importance is represented by the position of the voltammetric peak, rather than the magnitude of the wave. In the case of the metal-doped graphene modified electrodes, the larger peak current is likely due to a slightly larger surface area at the electrode (see **Table 4**).

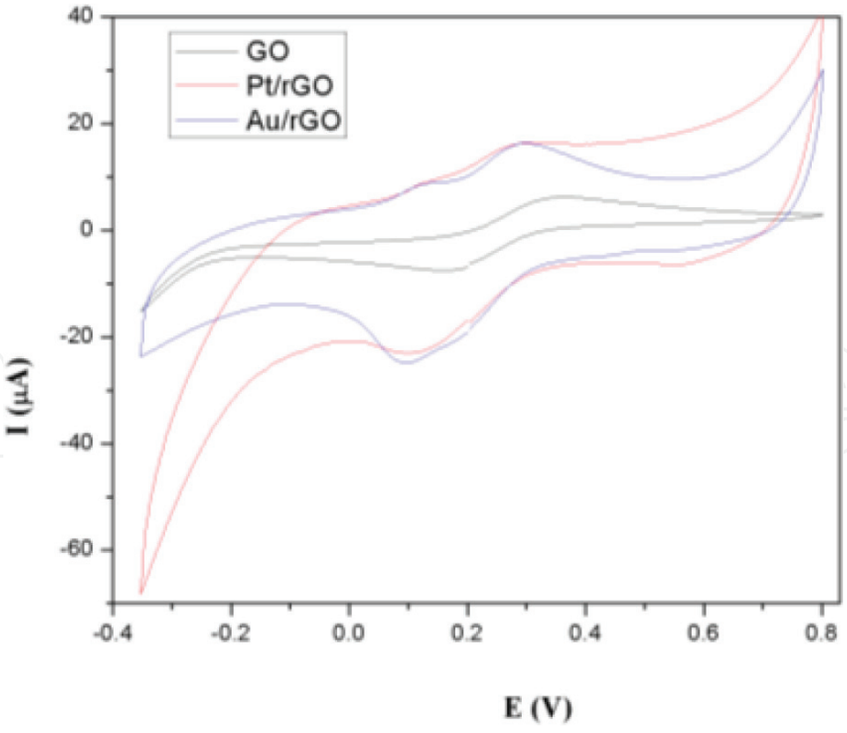

Figure 14. Overlay of the cyclic voltammograms for GO, Pt-doped rGO and Au-doped rGO modified electrodes for the redox process of 1.0 mM $K_3Fe(CN)_6$ in 0.5 M KCl solution (v = 20 mV s^{-1}).

In order to better investigate the electroanalytical outcome of these graphene modified electrodes, we performed differential pulse voltammetry (DPV) measurements. The DPV experiments were meant to support the cyclic voltammetry investigations, as it is clearly known that DPV can assist in resolving the signals due to species with close half-wave potentials, as it measures the difference between two currents, before the end of the pulse and before its application. The strength of this technique is evident when poor electrochemical signals are obtained in cyclic voltammetry, enabling the registration of well-defined signals through the elimination of the non-Faradaic processes. Moreover, DPV provides useful information when the resolving of the voltammetric signals given by two species with close half-wave potentials is needed, producing easily quantifiable peak shaped responses.

Figure 15 compares the differential pulse voltammograms of the graphene modified carbon paste electrodes, as well as the classical glassy carbon electrode. In all cases, sharp and well-resolved peaks are observed. The anodic (right side) and cathodic (left side) peaks are higher for the metal-doped reduced graphene oxide modified electrodes with the highest peak current being observed for the gold doped reduced graphene oxide modified electrode. An important parameter of an electrode material is its electronic properties, namely, the density of electronic states (DOS). The DOS of graphene materials has been reported as being high and it can be increased by varying the amounts of loaded graphene. Gold has a DOS of 0.28 states atom^{-1} eV^{-1} with high conductivity due to high proportion of atomic orbitals. Thus, the Au-doped rGO modified electrodes are highly sensitive for electrochemical investigation of the ferri/ferro redox system.

The active surface areas of the graphene modified electrodes were estimated according to the slope of the I_a *vs.* square root of the scan rates plot for a 1.0 mM $K_3[Fe(CN)_6]$, solution using 0.50 M KCl electrolyte, according to Randles–Sevcik equation [16]:

$$I_a = 2.69 \cdot 10^5 \cdot n^{3/2} \cdot D^{1/2} \cdot A \cdot c \cdot v^{1/2} \quad (3)$$

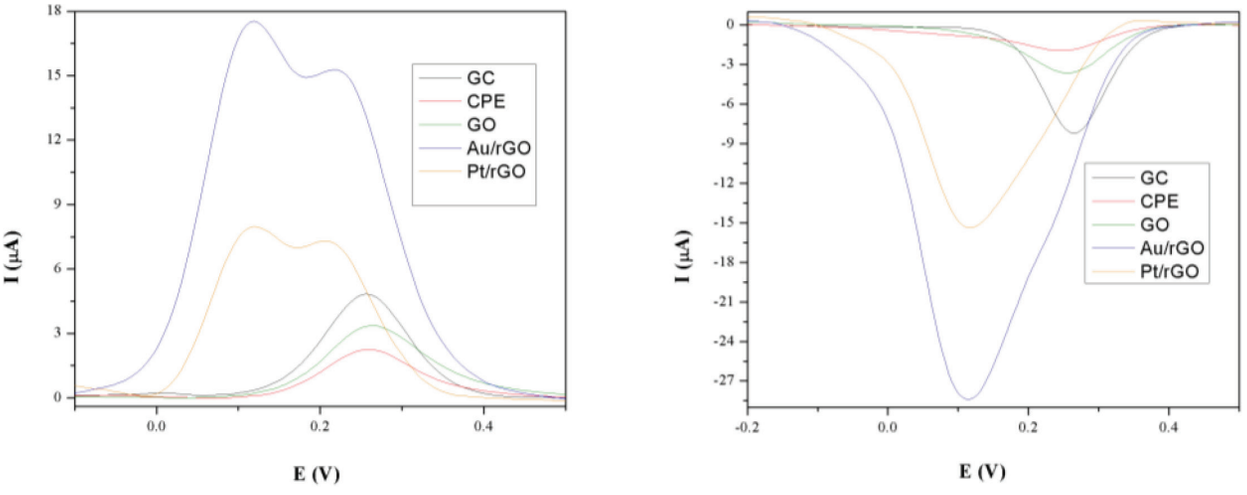

Figure 15. DPV voltammograms for graphene modified electrodes and commercially available glassy carbon electrode (GC): oxidation (left) and reduction (right) with optimized DPV parameters: modulation amplitude of 25 mV and step potential 5 mV.

http://dx.doi.org/10.5772/intechopen.80941

where I_a refers to the anodic peak current, n to the electron transfer number, A to the surface area of the electrode, D is the diffusion coefficient, c the concentration of $K_3[Fe(CN)_6]$ and ν is the scan rate.

For n = 1 and D = 6.68 × 10^{-6} cm^2 s^{-1} using the slope of the Ip–$\nu^{1/2}$ relation, the microscopic areas were calculated for all the used modified electrodes. The results show that metal-doped graphene oxide materials cause an increase in the active surface of the electrode. The comparison between modified GO electrode and Au-doped rGO reveals a higher active surface of the latter electrode which recommends this material as an electrocatalyst for the ORR reaction in fuel cells. Also, the Pt-doped rGO modified electrode exhibits an electrode active surface two times higher than the graphene oxide modified electrode.

Under PEMFC conditions at cell voltage of around 1.0 V during no-load, the Pt metal dissolution is expected. Moreover, Pt oxides are produced at potentials higher than 0.6 V_{SHE}. In particularly at potentials above 0.95 V_{SHE}, oxygen atoms can replace Pt atoms, thus the potential cycling cause remarkable changes of the catalyst structure. The catalyst exposure to such an accelerated test namely the potential cycling between 0.0–1.2 V_{SHE} lead to a fast catalyst aging, opposed to the constant potential holding test [17]. Thus, the potential cycling could be used as simultaneous CV characterization and degradation testing tool.

For this purpose, the in-situ electrochemical evaluation was performed in a single fuel cell system PEMFC with active area of 25 cm^2 (ElectroChem, USA). A detailed description of the electrodes and membrane electrode assembly fabrication procedure was reported in our previous studies [11–13]. For actual study, the Pt loading was established at 0.2 mg_{Pt} cm^{-2} for anode of all developed fuel cells. The cathode catalyst layer was modified by taking into account three FC configurations, as follows: deposition of commercial Pt/C catalyst Hispec 4000 with 0.4 mg_{Pt} cm^{-2} loading (case 1); commercial Pt/C 0.2 mg_{Pt} cm^{-2} and Pt/rGO with 0.2 mg_{Pt} cm^{-2} loading (case 2); commercial Pt/C 0.2 mg_{Pt} cm^{-2} and Au/rGO with 0.2 mg_{Au} cm^{-2} loading (case 3).The fuel cell test station included specific devices such as configured workstation, fuel cell, DS electronic load, bubble-type humidifiers. The PEMFC was operated at 0.7 V for 1 h for membrane electrode assembly conditioning. After steady state operating conditions were maintained, the cyclic voltammetry measurements were performed in a H_2/N_2 mode cell, from 0.025 to 1.2 V at a scan rate of 0.05 V/s. The flow rates of reactants (50 and 150 mL min^{-1}) gases (H_2 and N_2) were adjusted using flow controllers. The cell temperature and pressure were fixed at 70°C and 1 bar pressure. The developed control system based on NI c-RIO hardware was used to control the PEMFC system.

Carbon corrosion causes the detachment of metal nanoparticles and thus electrical isolation and electrocatalytic inactivity. Taking into account the instabilities due to catalyst support which lead to diminishing of FC performance, we investigated the support aging. **Figures 16–18** present the cyclic voltammograms before and catalyst exposure to 2000 cycles between 0.025 and 1.2 V potential cycling. Our preliminary results indicated that the oxidation and reduction signals approx at 0.025–0.3 V decreased differently after accelerated test, indicating the loss in electrochemical surface area for all cases, more pronounced being recorded for commercial catalyst. In case 1 it is easily to observe the change in hydrogen adsorption/desorption on Pt both for hydrogen oxidation and hydrogen reduction. In case 2 and 3, insignificant changes

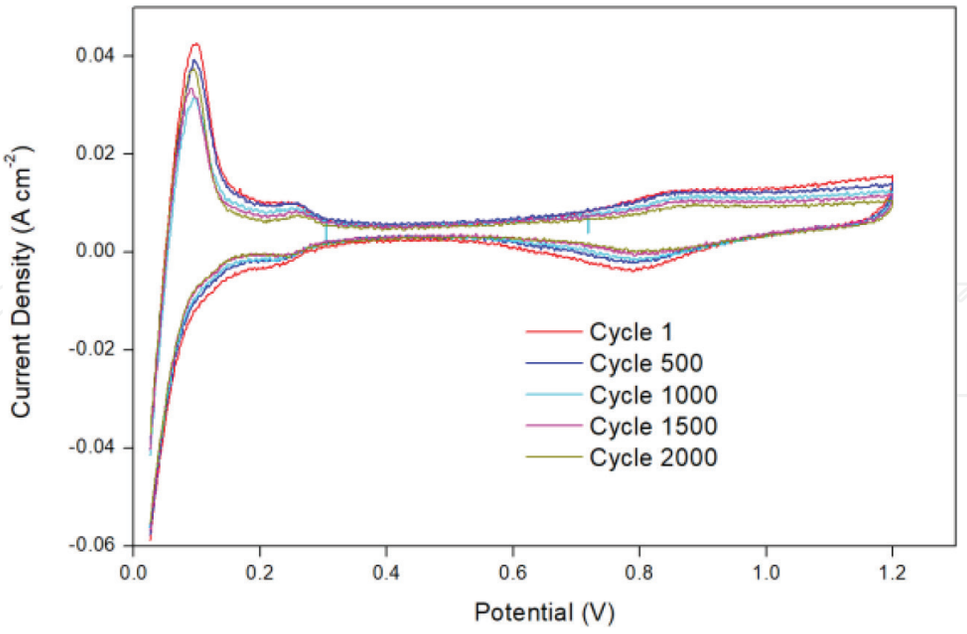

Figure 16. Cyclic voltammetry of commercial Pt/C for 2000 cycles in following operation conditions: temperature 70°C; scan rate 50 mV/s.

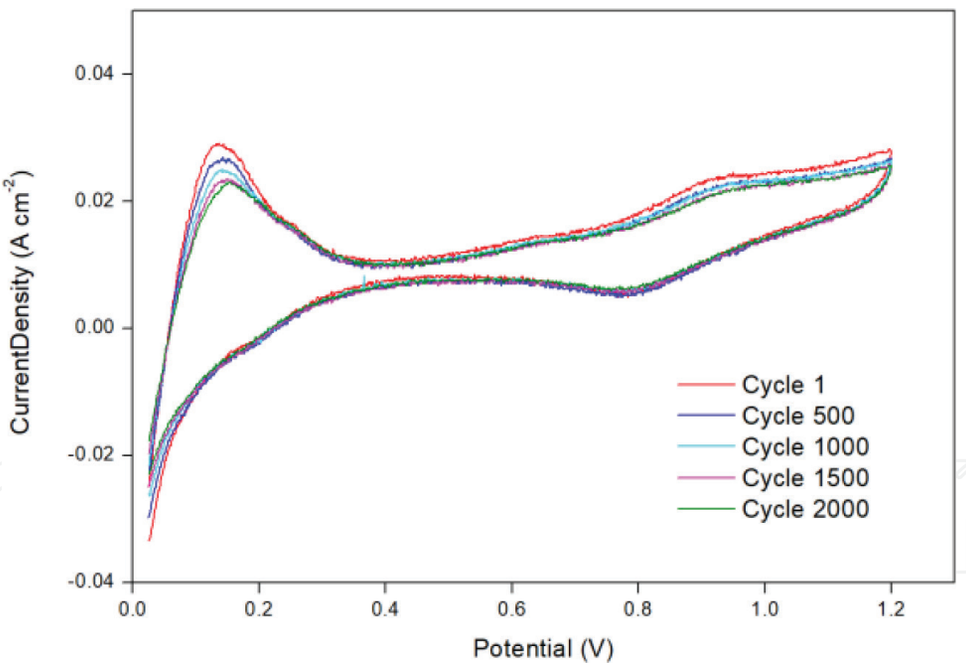

Figure 17. Cyclic voltammetry of Pt/rGO for 2000 cycles in following operation conditions: temperature 70°C; scan rate 50 mV/s.

were observed for reduction signal, which recommend Pt- and Au-doped rGO as potential ORR catalyst for a more comprehensive investigation.

Clearly, there are many types of GO modified electrodes and each is performing for different redox system, but the electrochemistry of graphene materials is far from being fully explored.

http://dx.doi.org/10.5772/intechopen.80941

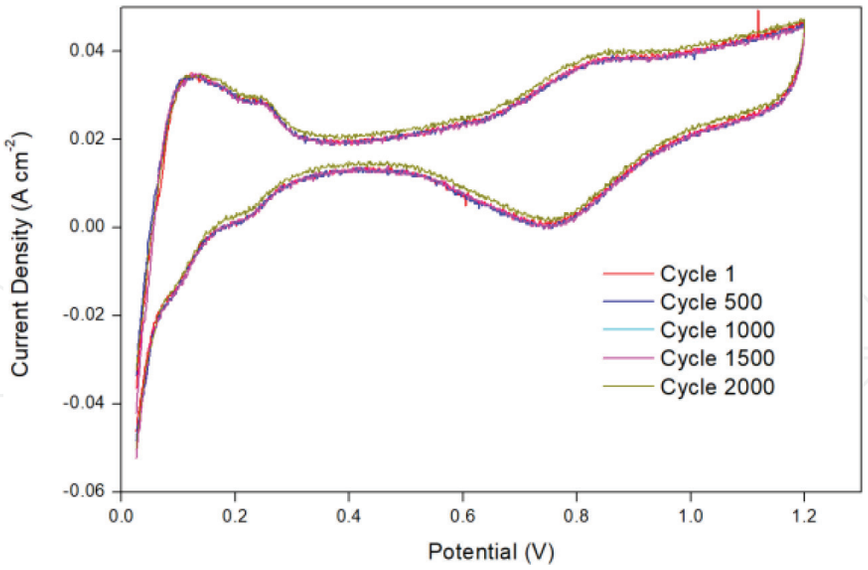

Figure 18. Cyclic voltammetry of Au/rGO for 2000 cycles in following operation conditions: temperature 70°C; scan rate 50 mV/s.

The graphene based material modified electrodes presented herein can significantly contribute to the fundamental understanding of graphene electrochemistry and its application as an electrode material. Future work can be directed to exploring these modified electrodes towards the application of graphene materials in ORR reactions for the development of performing fuel cells.

4. Conclusions

In conclusion, we have successfully synthesized PtNP/rGO and Au NP/rGO nanomaterials. The successful incorporation of Au and Pt nanoparticles into the graphene oxide structure was confirmed. SEM and STEM images show the good spatial distribution of metal nanoparticles onto the layered graphene sheets. Electrocatalytic performance of the prepared materials towards the ORR reaction using cyclic voltammetry and differential pulse voltammetry show that metal-doped graphene oxide materials caused an increase in the active surface of the electrodes. The results obtained by electrochemical characterizations suggest that metal-dispersed nanoparticles on reduced graphene oxide holds a great application potential as a promising electrocatalyst for oxygen reduction reaction due to the advantages of facile preparation and increased catalytic performance. It can be anticipated that the PtNP/rGO and AuNP/rGO composite materials hold great potential for developing novel ORR electrodes for PEM fuel cells. This imparts a high level of confidence that the materials developed as ORR electrocatalysts will be used in our future studies for the fabrication of cathodes for PEM fuel cell, the goal being the improvement of the fuel cell in terms of performance, life time and durability. Therefore, the reason for designed ORR electrocatalyst involves the advantage of improved catalytic activity due to the incorporation of a noble metal (platinum/gold) and ameliorated durability from the 1-dimensional structure.

Acknowledgements

This work is supported by the Ministry of Research and Innovation from Romania by the National Plan of R&D, Project No. PN 18 12 01 02, PN 18 12 01 04 and by Executive Agency for Higher Education, Research, Development and Innovation, under Project M-ERA.net 37/2016. The authors wish to thank Dr. Izabela Jinga from the Centre of Organic Chemistry 'Costin D. Nenitescu' Romanian Academy for her work in the electrochemical experimental study.

Conflict of interest

The authors declare that there is no conflict of interest.

Author details

Adriana Marinoiu[1]*, Mircea Raceanu[1], Elena Carcadea[1], Aida Pantazi[2], Raluca Mesterca[2], Oana Tutunaru[2], Simona Nica[3], Daniela Bala[4], Mihai Varlam[1] and Marius Enachescu[2]

*Address all correspondence to: adriana.marinoiu@icsi.ro

1 RD Institute for Cryogenics and Isotopic Technologies—ICSI, Rm Valcea, Romania

2 Center for Surface Science and Nanotechnology, Politehnica University of Bucharest, Romania

3 Centre of Organic Chemistry 'Costin D. Nenitescu' Romanian Academy, Romania

4 Department of Physical Chemistry, Faculty of Chemistry, University of Bucharest, Romania

References

[1] Gasteiger HA, Marković NM. Just a dream—Or future reality? Science. 2009;**324**(5923): 48-49. DOI: 10.1126/science.1172083

[2] Zhu C, Dong S. Recent progress in graphene-based nanomaterials as advanced electrocatalysts towards oxygen reduction reaction. Nanoscale. 2013;**5**:1753-1767. DOI: 10.1039/C2NR33839D

[3] Lale IS et al. Engineered catalyst layer design with graphene-carbon black hybrid supports for enhanced platinum utilization in PEM fuel cell. International Journal of Hydrogen Energy. 2017;**42**(2):1085-1092. DOI: 10.1016/j.ijhydene.2016.08.210

[4] Shuo D, Anli S, Li T, Wang S. Molecular doping of graphene as metal-free electrocatalyst for oxygen reduction reaction. Chemical Communications. 2014;**50**:10672-10675. DOI: 10.1039/C4CC05055J

[5] Li M, Zhang L, Xu Q, Niu J, Xia Z. N-doped graphene as catalysts for oxygen reduction and oxygen evolution reactions: Theoretical considerations. Journal of Catalysis. 2014;**314**:66-72. DOI: 10.1016/j.jcat.2014.03.011

[6] Agnoli S, Favaro M. Doping graphene with boron: A review of synthesis methods, physicochemical characterization, and emerging applications. Journal of Materials Chemistry A. 2016;**4**:5002-5025. DOI: 10.1039/C5TA10599D

[7] Jiang L, Fan Z. Design of advanced porous graphene materials: From graphene nanomesh to 3D architectures. Nanoscale. 2014;**6**:1922-1945. DOI: 10.1039/C3NR04555B

[8] Yanan T, Zongxian Y, Xianqi D. Trapping of metal atoms in the defects on graphene. The Journal of Chemical Physics. 2011;**135**:224704. DOI: 10.1063/1.3666849

[9] Marinoiu A, Cobzaru C, Carcadea E, Raceanu M, Atkinson I, Varlam M, et al. An experimental approach for finding low cost alternative support material in PEM fuel cells. Revue Roumaine de Chimie. 2016;**61**(4-5):433-440

[10] Marinoiu A, Teodorescu C, Carcadea E, Raceanu M, Varlam M, Cobzaru C, et al. Convenient graphene based materials as potential candidates for low cost fuel cell catalysts. Reaction Kinetics Mechanisms and Catalysis. 2016;**118**:281-296. DOI: 10.1007/s11144-016-1016-7

[11] Marinoiu A, Raceanu M, Carcadea E, Varlam M, Stefanescu I. Doped Graphene as non-metallic catalyst for fuel cells. Materials Science. 2017;**23**:108-113. DOI: 10.5755/j01.ms.23.2.16216

[12] Marinoiu A, Raceanu M, Carcadea E, Varlam M, Balan D, Ion-Ebrasu D, et al. Iodine-doped graphene for enhanced electrocatalytic oxygen reduction reaction in proton exchange membrane fuel cell applications. Journal of Electrochemical Energy Conversion and Storage. 2017;**14**:31001. DOI: 10.1115/1.4036684

[13] Marinoiu A, Raceanu M, Carcadea E, Varlam M, Stefanescu I. Low cost iodine intercalated graphene for fuel cells electrodes. Applied Surface Science. 2017;**424**:93-100. DOI: 10.1016/j.apsusc.2017.01.295

[14] Sun CL, Lee HH, Yang JM, Wu CC. The simultaneous electrochemical detection of ascorbic acid, dopamine, and uric acid using graphene/size-selected Pt nanocomposites. Biosensors & Bioelectronics. 2011;**26**:3450. DOI: 10.1016/j.apsusc.2017.01.295

[15] Lin WJ, Liao CS, Jhang JH, Tsai YC. Graphene modified basal and edge plane pyrolytic graphite electrodes for electrocatalytic oxidation of hydrogen peroxide and β-nicotinamide adenine dinucleotide. Electrochemistry Communications. 2009;**11**:2153

[16] Bard AJ, Faulkner LR. Electrochemical Methods. New York: Wiley; 1980

[17] Dana S, Hulstede J, Wagner P, Kruusenberg I, Tommeveski K, Dyck A, et al. Stability of Pt nanoparticles on alternative carbon supports for oxygen reduction reaction. Journal of the Electrochemical Society. 2017;**164**:995

IntechOpen